Energy & Buildings 174 (2018) 452–463

Contents lists available at ScienceDirect

Energy & Buildings

journal homepage: www.elsevier.com/locate/enbuild

Calculation of the external surface temperature of a multi-layer wall considering solar radiation effects

Beatriz M. Marino, Natalia Muñoz, Luis P. Thomas*

Geophysical and Environmental Flows Group, Centro de Investigaciones en Física e Ingeniería del Centro Provincia Buenos Aires, CONICET – Universidad Nacional del Centro Provincia Buenos Aires – CICPBA, Pinto 399, Tandil 7000, Argentina

ARTICLE INFO

Article history:
Received 24 January 2018
Revised 22 June 2018
Accepted 3 July 2018
Available online 9 July 2018

Keywords:
Infrared thermography
External surface temperature
Solar radiation effects
Sol-air temperature
Non-steady state heat flux

ABSTRACT

Infrared thermography has become a valuable tool for providing reliable information on the constructive components of the envelope of existing buildings and for checking if the thermal behaviour of a construction is consistent with the design parameters. However, infrared thermography has a limited capacity to offer quantitative accurate experimental results when the solar radiation incident on the facades is significant. The current study presents a methodology for theoretically calculating the external surface temperature of a multi-layer wall exposed to diurnal variations of the external environment temperature, which are caused by solar warming, hence validating a set of in situ measurements conducted using a thermographic camera over a time interval of interest. The measured external surface temperature is related to the theoretical equivalent sol-air temperature and the external and internal air temperatures by the numerical solution of the heat equation that is used to estimate the heat flux through a non-homogeneous medium. In addition, the numerical results are successfully compared with those obtained using the analytical standard admittance method. Thus, the instantaneous measurements of the external surface temperature can be generalised to calculate the heat flux into the building while considering the solar radiation effects during extended periods of time.

1. Introduction

Having efficient energy management of constructions depends on the understanding of the heat transfer mechanisms through the building envelope, particularly the heat flux q (W/m^2) transferred by conduction. Therefore, urban aspects (e.g. building orientation and location), variations of environmental factors (e.g. temperature, solar radiation, wind and activity of occupants) and the thermal properties of the materials that make up the walls (e.g. heat transfer coefficient and thermal transmittance) are incorporated into the building design to optimise the hygro-thermal comfort, reduce the energy consumption and improve the indoor lighting and air quality. Once q has been determined, it is possible to choose and arrange the air-conditioning systems to anticipate costs during the design stage or decide the appropriate changes in buildings under actual use conditions to encourage energy savings. But during the design phase, the heat exchange between the interior and exterior is assessed by considering the base values suggested by technical standards (e.g. ISO, ASHRAE, CIBSE, IRAM in Argentina) and spreadsheets that facilitate arithmetic operations [1–3], the assessment of existing buildings is also based on theoretical and/or numerical results. It is important to note here that the thermal behaviour of a building is often underestimated or neglected during its construction and operation stages, mainly because building elements may not perform as expected when they are in situ [4–6]. The detection of cold and warm zones associated with heat losses and gains, respectively, is also important. Although the direct heat gains through glazing surfaces are often considered in the calculations, the same does not apply, however, to the effect of the solar radiation that heats the opaque facades of the building envelope and increases the flux q through them. Hence, the estimate of q also requires meteorological databases and the knowledge of the conditions maintained inside the building over long periods of time.

Other factors, such as the impact of the surrounding vegetation and the shadow of the neighbouring premises at certain times of the day, are rarely considered in the simplest models, thus underestimating some significant parameters needed to perform a correct thermal assessment of buildings. In addition, the relevance of the thermal surface resistances of the building envelope is often underestimated regarding, for example, the effect of the parasols and porches on the houses to reduce the incidence of sunlight in summer [1,7–8]. This is probably because the estimation of the sur-

* Corresponding author.
E-mail addresses: bmarino@exa.unicen.edu.ar (B.M. Marino), nmunoz@exa.unicen.edu.ar (N. Muñoz), lthomas@exa.unicen.edu.ar (L.P. Thomas).

https://doi.org/10.1016/j.enbuild.2018.07.008
0378-7788/

Nomenclature

c	diffusion number
C_p	specific heat (J/kgK)
D	thermal diffusivity (m^2/s)
f	decrement factor
h	convective coefficient (W/m^2K)
I_t	total solar irradiance
ℓ	wall width
N	number of layers that compose the wall
q	heat flux through a wall (W/m^2)
q_1	heat flux incoming to the building envelope (W/m^2)
q_2	heat flux outgoing from the building envelope (W/m^2)
q_e	heat flux through the external air boundary layer (W/m^2)
q_{ss}	steady-state heat flux (W/m^2)
R_{se}	external surface thermal resistance (m^2K/W)
R_{si}	internal surface thermal resistance (m^2K/W)
t	time (h)
T	temperature (°C)
T_e	external environment temperature (°C)
T_i	internal environment temperature (°C)
$T_{sol\text{-}air}$	equivalent sol-air temperature (°C)
T_{se}	external surface temperature (°C)
T_{si}	internal surface temperature (°C)
U	overall heat transfer coefficient (W/m^2K)
u	dynamical transmittance (W/m^2K)
x	spatial coordinate (m)
X	spatial distribution of temperature
Y	admittance (W/m^2)

Greek letters

α	absorptivity
φ	time lag (h)
λ	thermal conductivity (W/m°C)
Θ	time distribution of temperature
ρ	density (kg/m^3)
τ	period
ω	angular frequency
ζ	phase

Subscripts

0	periodic function amplitude
e	external value
i	internal value
j	interface
s	value on a surface
ss	steady-state regime

face resistances depends not only on the temperature and humidity differences but also on the wind, shape of the envelope, surroundings trees, and so forth.

The current paper presents a methodology for theoretically estimating the external surface temperature of a wall while taking into account the solar radiation effects, thus validating the values measured with a thermographic camera. As a study case, a double brick wall with internal thermal insulation and low global thermal conductivity was chosen; therefore, it is expected that the variations of the flux q through the wall have a time lag with respect to the temperature variations. The wall is part of the envelope of a building under actual use conditions, faces northeast in the southern hemisphere and includes plane surfaces partially sheltered from the sun and cylindrical unsheltered surfaces. Thermographic measurements were performed at different times of the day (after dawn, at noon when the solar radiation effects are important and at dusk) and in every season of the year. The substantial number of in situ measurements compensates the deviations from the mean thermal behaviour caused by barely controllable parameters (e.g. wind and cloudiness). The temperature values obtained are related to the theoretical equivalent *sol-air temperature* $T_{sol\text{-}air}$ [9–12] and the internal and external environment temperatures by means of the numerical solution of the heat equation. Therefore, a series of thermographic measurements is generalised as a data time sequence to calculate the external real surface temperature of the building envelope while considering the wall heating caused by the solar radiation. In addition, valuable physical information about the heat transfer through the wall is evidenced in the process.

The paper is divided into the following parts. Section 2 provides a general overview of the usefulness of the thermographic technique and its contribution to the problem addressed in this study. Section 3 introduces the main analytical fundamentals of the methodology, including those associated with the heat transfer by conduction through a wall with variable surface temperatures and the corresponding numerical solution of the heat equation. Section 4 describes the measurements performed, while the results are presented in Section 5. Some remarks are offered in Section 6, and finally, the conclusions are given in Section 7.

2. State of the art

When under the steady-state hypothesis, which is not always fulfilled, the flux q is usually considered to be proportional to the difference between the internal (T_i) and external (T_e) air temperatures [13–16]. The proportional relationship is given by a key parameter for assessing the thermal quality of the building envelope: the overall heat transfer coefficient U (W/m^2K). The U-value depends on the thermal conductivity λ of the materials and the internal (R_{si}) and external (R_{se}) thermal surface resistances. In laboratory experiments, the employment of temperature sensors, heat flux meters (HFM) and infrared thermography (IRT) is useful to determine the thermal properties of the materials and hence the U-value. In particular, the non-invasive HFM method [17–18] presents some limitations for the in-situ measurement of the U-value: the test takes at least 72 h to execute, can only measure a local point of the wall, and the accuracy is poor; therefore, it is not reliable for non-homogeneous building elements [16]. Despite the simplicity of the methods for calculating the steady-state heat flux q_{ss}, they do not always describe the actual thermal behaviour of the construction, thus being inappropriate when diurnal variations of temperature are important [19–21].

To assess the effect of the time variations of q, in addition to U, it is necessary to know the density and specific heat of materials that compose the building envelope and solve the non-traditional heat equation [22–24]. The dynamical response of buildings to variations in the outside temperature can be determined by means of the dynamical transmittance u, in which case q is found by applying the *admittance method* introduced by Pipes [25], who used the analogy between the thermal problem solution and that of an electrical transmission line. Davis [26] developed this method for walls, introducing the admittance and calculation of complex numbers matrices and representing graphically the relationship between temperature and heat flux in the form of time-dependent vector diagrams (or *phasors*). For an unsteady-state heat flux through the envelope, the attenuation of the energy flux with the wall thickness (or decrement factor) and a time lag between the maximum values of the temperature difference and the heat fluxes at both sides of the wall must be considered.

Whatever way the heat transfer is analysed, the temperature values preferably obtained from in situ measurements are required. Quantitative IRT was successfully used to determine in situ U-

values, thermal bridges losses, surface thermal resistances and the moisture content in walls [13–16,27–28]. An interesting and critical review based on a wide range of recent advances on quantitative and qualitative uses of passive (or static) and active IRT was presented by Lucchi [29] (see also [30]). The techniques employed to measure the *U*-value of walls using IRT data are based on specific algorithms that consider the temperature difference between the internal and the external environment [27,31], the heat power through the envelope [13], calculations related to solar radiation [13,14,32], the thermal emissivity of walls [13–15,31], the reflected apparent temperature [14,15,31] and the wind speed [17]. The *U*-value is typically calculated as the ratio between the energy dissipated in the envelope and the difference between the inner and outer temperature. The energy dissipated by radiation is estimated by means of theoretical relationships using the surface temperature of the walls (measured using a thermographic camera) and the environment temperature. The calculation of the energy dissipated by convection uses the boundary layer convective coefficient, either the one recommended by technical standards or the one calculated employing formulas based on the wind speed. The inside IRT ensures acceptable results thanks to a reduction of the impact of boundary conditions, while the outside IRT requires the calculation of the external convective coefficient as a function of the weather conditions. A standard deviation of 25–35% is obtained between IRT measurements and theoretical *U*-values [33], and there is a standard deviation of 10–20% between the IRT and measured data [13,34], which increases up to 80% with wind velocities larger than 1 m/s [13]. Consequently, the precision of the *U*-value obtained depends critically on the thermographic measurements' accuracy. The emissivity, reflectance, surface roughness, walls moisture and weather conditions (solar radiation, cloud cover, direct sunlight, ambient temperature, relative humidity, wind speed and internal/external air temperature gradient) are potential sources of error in the surface temperature determination. To obtain comparable results when different operators and equipment are used and to reduce the impact of the above factors, the International Organization for Standardization and the American Society for Testing and Materials, among others, established procedures for infrared image capture and processing. To minimise errors in the *U*-value calculation, it is recommended that tests should be conducted: (i) preferably in the early morning before sunrise and/or in the evening after sunset to avoid solar radiation; (ii) with an internal and external temperature difference greater than 10 °C to allow for measurable heat exchange through the envelope; (iii) under low values of wind speed (smaller than 1.0 m/s) to avoid the effects of convective phenomena; and (iv) when the internal temperature have been stable for 48 h prior to the test. The latter requirement is because the flux q is attenuated through the envelope and delayed with respect to the T_e variations, especially through highly insulated walls.

3. Methodology description

The theoretical calculation of the external surface temperature T_{se} of a wall requires knowing the values of T_e and the total solar irradiance I_t (Wm^{-2}). These parameters can be related using whether the Boltzmann's equation (as done by, for example, Albatici and Tonelli [13], Evangelisti et al. [35], O'Grady et al. [36] and Tejedor et al. [16]) or the equivalent sol-air temperature $T_{\text{sol-air}}$ (as done by, for example, O'Callaghan and Probert [37] and Peng and Wu [38]). In the latter case, the temperature difference between both sides of the external air boundary layer, $T_{\text{sol-air}} - T_{se}$, is related to R_{se} and the heat flux q_e that crosses the boundary layer at time t in the following way:

$$q_e(t) = \frac{1}{R_{se}}[T_{sol-air}(t) - T_{se}(t)] \quad (1)$$

Table 1
Values of h_e for different standards.

Standards	$h_e = R_{se}^{-1}$ (W/m^2K)
IRAM 11601 (Argentina)	25
CIBSE (United Kingdom)	17
ASHRAE (United States of America)	22.7 (summer) – 34.0 (winter)
ENER (Mexico)	13

According to Eq. (1), $T_{\text{sol-air}} - T_{se}$ may be significant for large q_e, even when R_{se} is assumed constant, and can also change its sign depending on if the wall receives ($q_e > 0$) or dissipates ($q_e < 0$) heat. As seen in the following, the q_e-value is determined by solving the heat equation by considering the evolution of the real T_i and T_e temperatures and I_t irradiance.

The methodology developed is represented in the flowchart in Fig. 1. Essentially, it consists first of calculating I_t as indicated in Table 2 using building location data, (*Step 1*). Then, by using the measured temperatures T_i *and* T_e, $T_{\text{sol-air}}$ is estimated by means of Eq. (2) (*Step 2*). Moreover, the temperature distribution inside the wall caused by a sinusoidal variation of $T_{\text{sol-air}}$ is numerically simulated. Once the simulation code is validated by successfully comparing the numerical and theoretical results (the latter obtained by applying the admittance method as indicated in Section 3.2), the evolution of the heat flux q and temperature T through the wall can be numerically simulated using the actual variation of $T_{\text{sol-air}}$ (*Step 3*) as described in Section 3.3. Next, T_{se} is determined using Eq. (1) (*Step 4*). Finally, the theoretical values for T_{se} are compared with those provided by the IRT technique (*Step 5*). If they coincide, $T_{se} = T_{se}(t)$ is obtained (*Step 6*).

3.1. Calculation of the sol-air temperature

The opaque elements of the envelope capture energy from the sun, heating the building's external surface at temperature T_{se}. The absorbed energy is partly re-emitted in the form of thermal radiation to the environment, although this fraction of energy is significantly less than the total absorbed energy and is partly compensated by the thermal radiation emitted by the surrounding buildings, so that it is usually neglected in the calculations. The increase of the heat flux as a result of solar irradiance can be included in the T_{se} calculation by means of $T_{\text{sol-air}}$. This is the outside air temperature for which, in the absence of radiation, the external environment delivers the same heat flux to the wall surface. If the radiation emitted by the envelope surface is negligible, it results in the following:

$$T_{sol-air} = T_e + \frac{\alpha I_t}{h_e}, \quad (2)$$

where α is the material absorptivity, and $h_e = R_{se}^{-1}$ is the boundary layer heat transfer coefficient. The value of I_t depends on the building's geographical location, the sun position in the sky and the façade's orientation. To calculate $T_{\text{sol-air}}$, in the first approximation, $h_e = 25\,W/m^2K$ is taken, which is provided by the technical standard IRAM 11601 (Table 1). It should be noted, however, that the effect of I_t on the q_e calculations with Eqs. (1) and (2) does not depend on the adopted value of h_e.

Table 2 shows the parameters and equations involved in the calculation of the corresponding $T_{\text{sol-air}}$ conducted in 2014. The radiation received in a given location depends on its longitude *LON* and latitude *LAT* and hour of the day. Time refers to the sun's position in the horizon and is independent of local time conventions (e.g. summer time, winter time, etc.). For doing this, the local solar time *LST* and the apparent solar time *AST* are used. *LST* is defined as when the sun is highest in the sky and is independent of the time variations between two successive passages of the sun

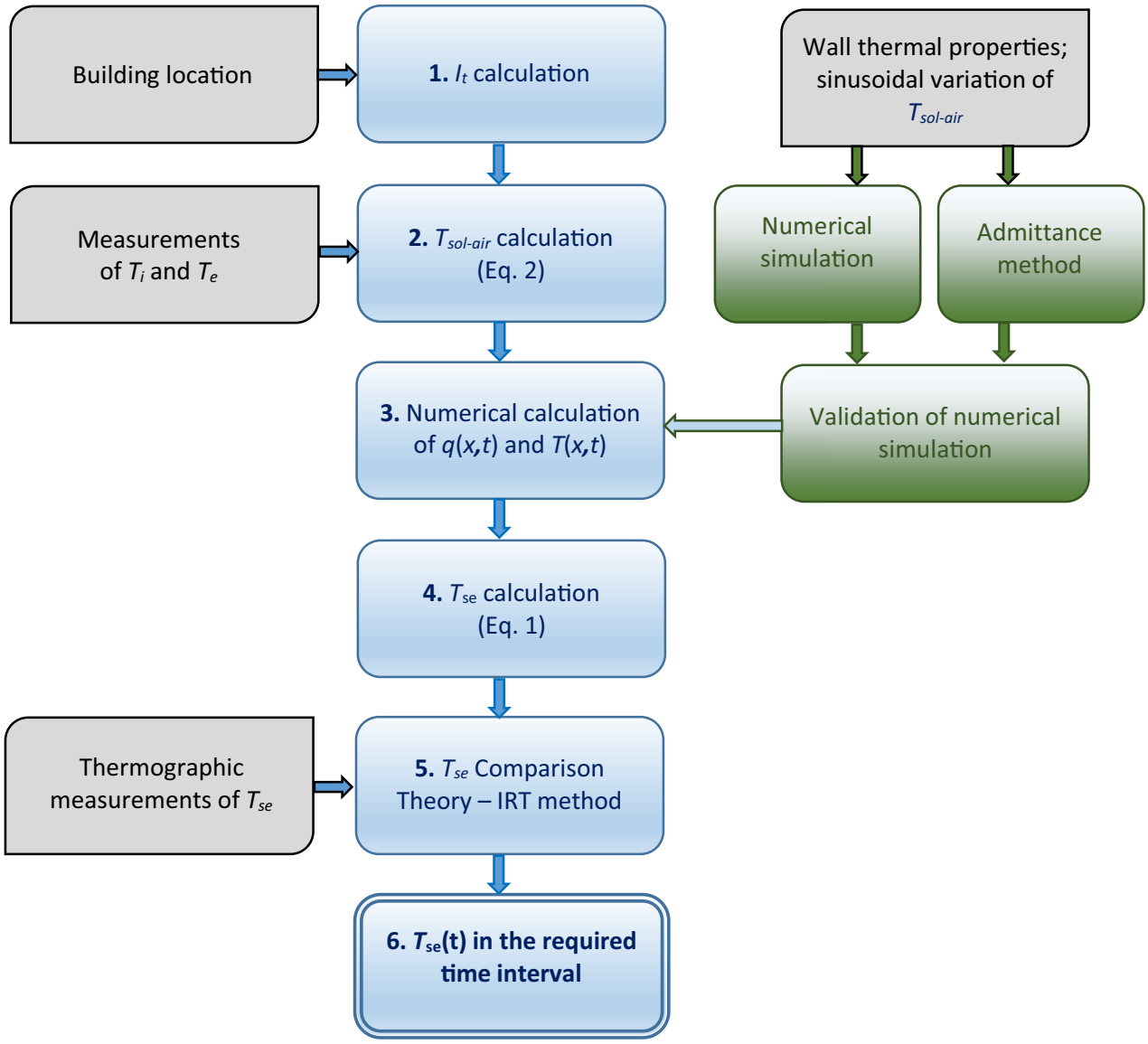

Fig. 1. Flowchart of the methodology.

across the same meridian; consequently, the day's length is constant throughout the year. *AST* is the interval between two successive returns of the sun to the local meridian. Because the earth's orbital velocity varies throughout the year, *AST* also varies somewhat from the mean time kept by a clock running at a uniform rate. This time difference between *AST* and *LST* is called the equation of time *ET* and varies between −14 and 16 min throughout the year (every year is different because of the sum of one day in leap years). In addition to the correct calculation of time, the sun must be located properly. The hour angle H is the angular displacement of the sun east or west of the local meridian due to the rotation of the earth and is measured in degrees or hours (1 h = 15°). H is zero at solar noon (about local time = 13:00 h, $AST \approx 12$ h), positive in the afternoon and negative in the morning. The solar declination δ is the angle between the earth–sun line and the equatorial plane, and it varies throughout the year between −23.45° during the summer solstice (21–22 December) and +23.45° during the winter solstice (21–22 June). The sun's position in the sky is conveniently expressed in terms of the solar altitude above the horizontal and the solar azimuth measured from the south. The solar altitude angle β is the angle between the horizontal plane and a line emanating from the sun. Its value ranges from 0° when the sun is on the horizon to 90° if the sun is directly overhead; negative values correspond to night times. The solar azimuth angle ϕ is the angular displacement from south of the projection on the horizontal plane of the earth–sun line. By convention, it is positive for afternoon hours and negative for morning hours.

3.2. . Calculation of the heat flux through a wall with variable surface temperatures

Consider a one-dimensional heat flow per unit area q transferred by conduction through a wall that consists of a non-homogeneous material between $x = 0$ (side 1, exterior) and $x = \ell$ (side 2, interior). Because these boundary conditions (BC) are defined for all time t, the heat equation can be solved by means of the method of separation of variables (or Fourier method); thus, the temperature is given as the product of two functions, each of which depends on one variable: $T(x,t) = X(x)\Theta(t)$. If the temperature difference between sides 1 and 2 varies periodically with time, period τ and angular frequency $\omega = 2\pi/\tau$, then $\Theta(t) = e^{i\omega t}$ and the

Table 2
Definitions of parameters and constants employed in the calculation of $T_{sol\text{-}air}$ for Tandil City [39,40].

Symbol	Description	Values / Equations (units)
LON	Longitude	59.1°
LAT	Latitude	−37.2°
ρ_g	Solar reflectance of the ground	0.2
GMT	Greenwich Mean Time	−03:00 h
SLT	Standard Local Time	45° (GTM × 15) (h)
C	Diffuse air coefficient	0.136 June, 0.073 October, 0.071 March
Σ	Surface tilt angle	90° = vertical, 0° = horizontal
AST	Apparent Solar Time	$AST = LST + ET/60 + (SLT - LON)/15$ (h)
ET	Equation of Time	$ET = 229.18[0.00075 + 0.019cos(0.493\text{d}) - 0.032sen(0.493d) - 0.015cos(1.972d) - 0.041sen(1.973)]$ (min)
LST	Local Solar Time	$LST = (LT - ET)$ (h)
LT	Local Time	0 – 24 (h)
d	Day of the year	0 – 365
H	Hour angle	$H = 15°(AST - 12)$ (°)
δ	Solar declination angle	$\delta = 23.45°\text{sen}[360(284 + d)/365]$ (°)
β	Solar altitude Angle	$\beta = \text{sen}^{-1}$ [cosLAT cosδ cos$H$ + senLAT senδ] (°)
ϕ	Solar azimuth Angle	$\phi = \cos^{-1}$ [(senβ senLAT − senδ)/(cosβ cosLAT)] (°)
γ	Surface-solar azimuth angle	$\gamma = \phi - \psi$ (°)
ψ	Surface azimuth angle	N: 180°; NE: −135°; E: −90°; SE: −45°; S: 0°; SW: 45°; W: 90°; NW: 135°
θ	Angle of incidence	$\theta = \cos^{-1}$ (cosβ cosγ senΣ + sinβ cosΣ) (°)
I_{DN}	Direct normal irradiance	$I_{DN} = E_0 e^{-B/\sin\beta}$ (W/m²) E_0: extra-terrestrial solar irradiance B: Apparent atmospheric extinction coefficient $e^{-B/\sin\beta}$: attenuation by the local atmosphere
I_D	Direct solar irradiance	$I_D = I_{DN}\cos\theta$ (W/m²)
Y	Ratio of clear-sky diffuse irradiance on a vertical surface to clear-sky diffuse irradiance on the horizontal	$Y = 0.55 + 0.437\cos\theta + 0.313\cos^2\theta$ (W/m²)
I_d	Diffuse horizontal irradiance measured on a horizontal surface	$I_d = C.Y.I_{DN}$ (W/m²)
I_{Earth}	Ground-reflected irradiance	$I_{Earth} = I_{DN}(C + \text{sen}\beta)\rho_g(1 - \cos\Sigma)/2$ (W/m²)
I_t	Total clear-sky irradiance	$I_t = I_D + I_d + I_{Earth}$ (W/m²)

function depending on the spatial variable is the solution of:

$$\frac{\partial T}{\partial t} - \frac{1}{\rho C_p}\frac{\partial}{\partial x}\left(\lambda\frac{\partial T}{\partial x}\right) = 0, \tag{3}$$

where $\rho(x)$ is the density, $C_p(x)$ is the specific heat, and $\lambda(x)$ is the thermal conductivity of the material. In the case of a homogeneous material, $\lambda = \text{const}$, and the known form of the heat equation is obtained:

$$\frac{\partial T}{\partial t} - D\frac{\partial^2 T}{\partial x^2} = 0, \tag{4}$$

where D is the thermal diffusivity of the material (m²/s), whose solution is:

$$X(x) = c_1\cosh(\gamma x) + c_2\sinh(\gamma x) \tag{5}$$

where c_1 and c_2 are constants, and:

$$\gamma = \frac{p(i+1)}{\ell} \quad \text{with} \quad p = \sqrt{\frac{\omega\ell^2}{2D}} \tag{6}$$

Assuming that the surface temperatures satisfy $T_{se} = T_{se0}e^{i\omega t}$ and $T_{si} = T_{si0}e^{i\omega t}$, it follows that $c_1 = T_{se0}$ and $c_2 = T_{si0} - T_{se0}\cosh(\gamma\ell)/\sinh(\gamma\ell)$. Because

$$q(x,t) = -\lambda\frac{\partial T(x,t)}{\partial x}, \tag{7}$$

which results in $q_1 = q_{10}e^{i\omega t}$ at surface 1 ($x = 0$) and $q_2 = q_{20}e^{i\omega t}$ at surface 2 ($x = \ell$), with

$$\begin{cases} q_{10} = b_{11}(T_{se0} - T_{si0}) \\ q_{20} = b_{21}(T_{se0} - T_{si0}) \end{cases} \tag{8}$$

The temperature T_{si0} is taken as a reference, while

$$b_{11} = \frac{\lambda}{\ell}p(i+1)\frac{\cosh[p(i+1)]}{\sinh[p(i+1)]} \quad \text{and}$$

$$b_{21} = \frac{\lambda}{\ell}p(i+1)\left\{\sinh[p(i+1)] - \frac{\cosh^2[p(i+1)]}{\sinh[p(i+1)]}\right\} \tag{9}$$

are complex numbers whose real part represents the amplitude of q variations, and the imaginary part represents the phase ζ with respect to T_{se} when the heat flux at side 1 is $q_1(t) = Re\{q_{10}\}\cos(\omega t + \zeta)$. For multi-layer walls, a complex numbers matrix is built for every layer, and the coefficients b_{11} and b_{12} over the entire wall width are calculated by multiplying the matrices [41]. This way of calculating the heat flux is known as the *admittance method* and is useful when sinusoidal variations of T_{se} and T_{si} are considered. To represent the real surface temperature variations using this method, Eqs. (7) – (9) should be employed for each component of the Fourier series expansion of T_{se}. However, in the current study, Eq. (3) is numerically solved while the admittance method is used to validate the results of the numerical simulation for simple sinusoidal variations with a period of 24 h (see Section 3.3).

The comfort condition implies that $T_i \approx 20$ °C while T_e–value depends on the local weather. Essentially, T_e shows seasonal ($\tau = 365$ days) and daily ($\tau = 1$ day) periodical variations, and other fluctuations associated with meteorological conditions. For the typical walls described in Section 4, it results $\omega\ell^2/2D << 1$ for $\tau = 365$ days and $\omega\ell^2/2D \approx 1$ for $\tau = 1$ day. This indicates that seasonal variations are slow and that the heat flux through the walls can be adjusted to the temperature variations experienced by the internal and external surfaces (i.e., an approximated steady-state condition is fulfilled), unlike the daily variations.

3.3. Numerical solution of the heat equation

The analytical solutions of the heat equation given by Eqs. (5)–(9) are valid in the event of sinusoidal variations of the internal and external temperatures. When such variations are not sinusoidal, the simplest procedure is to solve the heat equation numer-

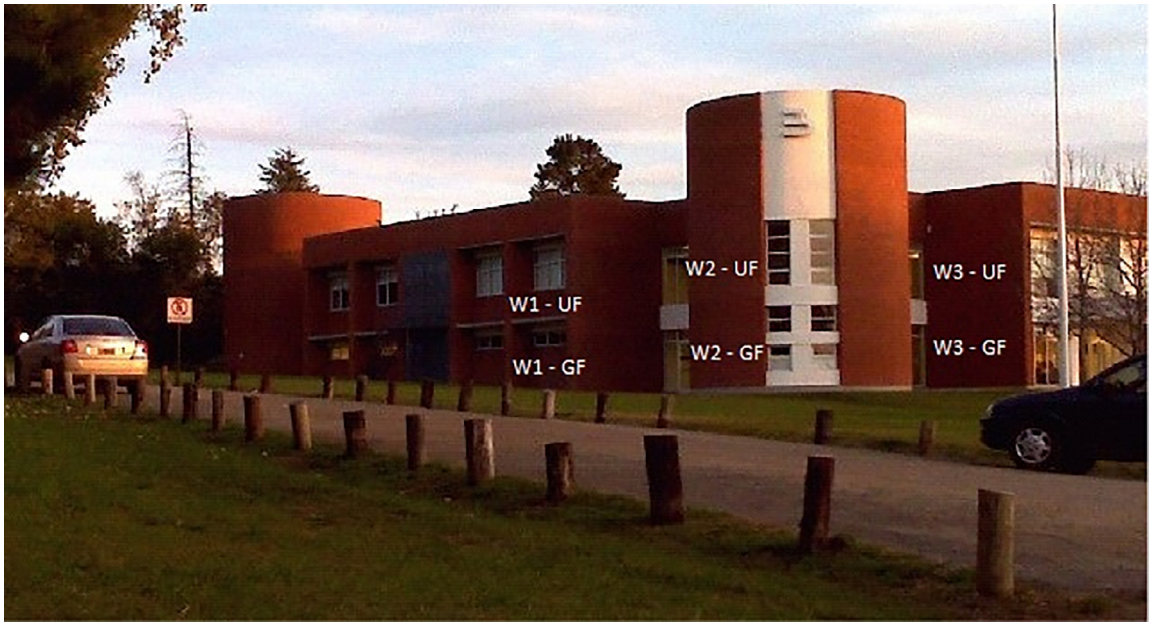

Fig. 2. Location of the assessed constructive sectors belonging to the northeast-facing facade of a typical construction in the centre of Buenos Aires province (Argentina).

ically. The resistances R_{se} and R_{si} that are associated with the heat transfer coefficients h_e and h_i, respectively, must be considered to choose the suitable BC. The flux q_e through the external air layer between the exterior at temperature $T_{\text{sol-air}}(t)$ and the external surface of the wall at temperature $T_{se}(t)$ is provided by Eq. (1). Similarly, the flux q_i through the internal air layer located between the interior at temperature $T_i(t)$ and the internal surface of the wall at temperature $T_{si}(t)$ is the following:

$$q_i(t) = \frac{1}{R_{si}}[T_{si}(t) - T_i(t)]. \tag{10}$$

Eq. (3) is parabolic and must be solved simultaneously in the entire spatial domain (i.e., along the entire width of the wall) and in the interval $0 < t < t_{end}$ under BC (1) and (10) [42]. Furthermore, the initial conditions (IC) affect the solution in the entire interval of calculation. The effect of an arbitrary IC on the solution can be neglected when considering the results found after a simulation time $t = 24$ h, as done in Section 5.

Eq. (3) is numerically solved by implementing the finite differences method programming in *MATLAB* [43,44]. It is a second-order method in space and explicit in time [42]. The wall of thickness ℓ is considered to be divided into N layers of equal thickness Δx. Temperatures T_j are defined in the $N+1$ interfaces between the different layers, while the material properties λ_j, C_{pj} and ρ_j ($j = 1$, 2, …, N) are defined at the centre of every layer. The numerical scheme is stable if the time step fulfils the following condition:

$$\Delta t \leq c\frac{(\Delta x)^2}{\lambda/\rho C_p}\bigg|_{\min}, \tag{11}$$

where $c < 0.5$ is the diffusion number, and *min* indicates the smallest value of the grid. Some alternative methods make it possible to avoid condition (11) such as, for example, the implicit numerical solution schemes of the time derivative and the Crank-Nicolson method [45].

4. Measurements

The assessed multi-layer walls belong to the northeast facing facade of a two-story building located in the semi-urban area of Tandil City (37°19′S–59°08′W, Buenos Aires Province, Argentina). The local climate is temperate and humid with mild summers, a daily thermal amplitude of 13–14 °C and annual temperature variations of the same value. The masonry consists of a solid brick wall 0.12 m thick and $\alpha = 0.95$, a panel of expanded polystyrene (EPS) 0.035 m thick, a waterproofing coating, a hollow brick wall 0.12 m thick and two layers of plaster on the inner side, fulfilling the local regulations for construction. All the walls of the building envelope are 0.30 m thick. The values of the thermal properties of the materials involved are shown in Table 3, together with the adopted values of R_{se} and R_{si} suggested by local technical standards. The envelope sectors that are analysed are identified as W1, W2 and W3 in Fig. 2 in both the upper floor (UF) and ground floor (GF); they receive an important (and similar) amount of solar radiation throughout the day.

The main technical characteristics of the measuring equipment are shown in Table 4. The temperature T_{se} was measured by employing the IRT technique. The equipment used in this work was a thermographic camera that captures the thermal radiation emitted or reflected by the surface of objects in the range $7.5 < \lambda < 14\,\mu$m, and proportionally transforms the energy received by each pixel in intensity. In this way, the corresponding temperature distribution is determined. The emissivity and the compensation for the reflected background temperature are determined according to Marino et al. [27]. Some measurements of the surface temperature were checked with a digital Smartmeter thermometer and a thermo-resistance PT-100 class 1/3, stuck to the surface. The thickness of walls and the distance (≈ 3 m) between the tested surface and the camera were measured with a laser distance meter.

Thermograms of the external wall sectors were acquired daily between 19 and 30 October 2015 (spring), 29 March and 7 April 2016 (autumn), 4 and 15 July 2016 (winter) and 29 November and 7 December 2016 (summer) at 7:15–8:00, 13:00–13:45 and 19:00–19:45. Measurements that were conducted in windy, rainy and/or foggy days were ruled out. The temperatures T_i in the GF and UF of the building were determined by averaging the data provided by two sensors placed in each floor. These sensors measure every 10 min. The temperature T_e and the irradiance I_t were measured by a weather station located 200 m from the building.

Table 3
Properties of the wall materials and surface thermal resistances values.

	R (m^2K/W)	ε (m)	λ (W/m °C)	ρ (kg/m^3)	C_p (J/kgK)	D (m^2/s)
R_{se}	0.04					
Solid brick	0.15	0.120	0.81	1600	1000	5.1×10^{-7}
EPS	1.00	0.0370	0.037	17	1700	1.3×10^{-6}
Hollow brick	0.40	0.120	0.30	800	920	4.5×10^{-7}
Thick coat of plaster	0.02	0.020	0.93	1400	1050	6.3×10^{-7}
Thin coat of plaster	0.01	0.005	0.70	1400	1012	4.9×10^{-7}
R_{si}	0.13					
Total	$R_t = 1.75$	$\ell = 0.30$				

Table 4
Main technical specifications of the equipment.

Equipment	Variable measured	Measuring range	Resolution	Accuracy/Precision
Infrared camera: FLUKE TiR32	Temperature	−20 °C to +150 °C	320 × 240 pixels	±2 °C or 2%
Digital thermometer: Smartmeter	Temperature	−200 °C to +600 °C	0.02 °C	±0.1 °C
Laser meter: FLUKE 414D	Distance	50 m	10^{-3} m	$\pm 2 \times 10^{-3}$ m
Temperature sensor: HOBO U12	Temperature	−20 °C to +70 °C	0.03 °C at 25 °C	±0.35 °C
Weather station: Decagon Em50	Temperature (T_e) - Irradiance (I_t)	−40 °C to +120 °C - 0 to 1750 Wm^{-2}	0.01 °C - 0.05 Wm^{-2}	±0.3 °C - ±0.05 Wm^{-2}

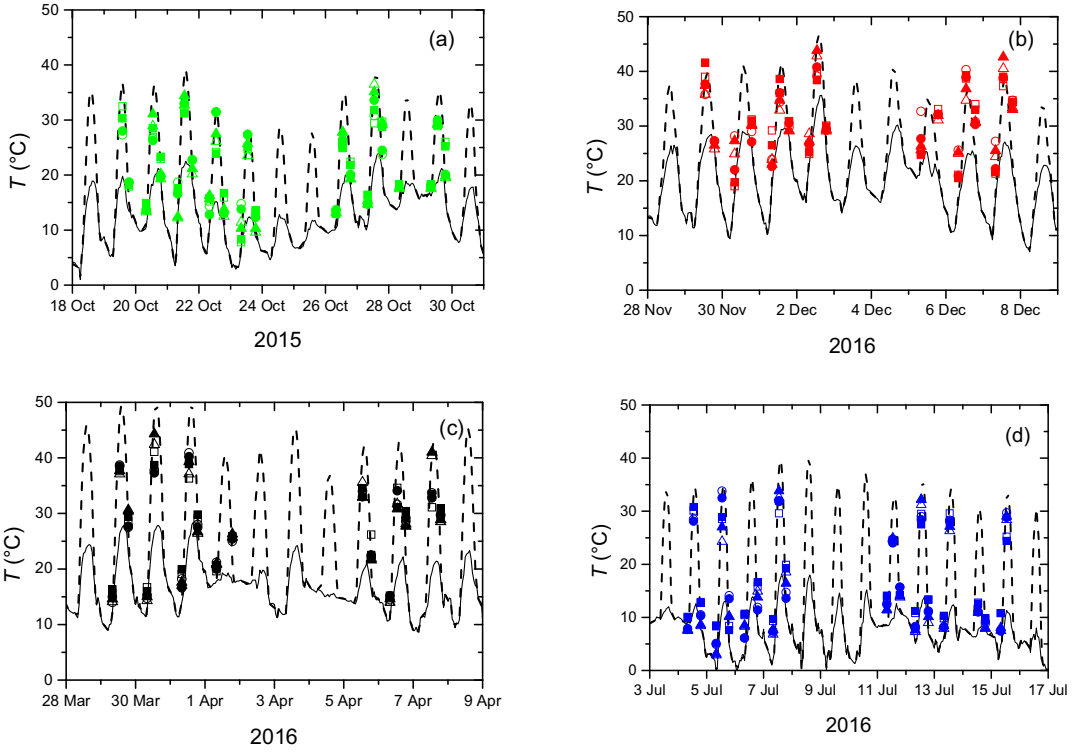

Fig. 3. Evolution of T_e (solid lines) and $T_{sol\text{-}air}$ (dashed lines) in spring (a), summer (b), autumn (c) and winter (d). The symbols represent the measurements of T_{se} corresponding to the wall sectors W1 (squares), W2 (circles) and W3 (triangles) in both GF (closed symbols) and UF (open symbols).

5. Results

5.1. Determination of temperatures T_{se} and $T_{sol\text{-}air}$

The symbols in Fig. 3 represent the temperature T_{se} measured with the thermographic camera in the wall sectors W1, W2 and W3 at GF and UF over the measuring intervals. These measurements are compared with the evolution of $T_{sol\text{-}air}$ obtained analytically (Section 3.1) and T_e provided by the weather station (Step 5, Fig. 1). The differences between $T_{sol\text{-}air}$ and T_e are important, especially around midday in winter, spring and autumn ($\Delta T_{max} = [T_{sol\text{-}air} - T_e]_{max} \approx 22$ °C in winter - Fig. 3d; $\Delta T_{max} \approx 12$ °C in summer - Fig. 3b). ΔT_{max} changes with the seasons because of the variations of I_t and the incidence angle θ of the solar beams on a vertical wall at the construction site. For a wall facing the northeast at the latitude 37.32°S, the solar beams fall almost tangentially on the wall in summer and almost perpendicularly at midday in winter, resulting in a higher incidence of solar radiation in winter. $T_{sol\text{-}air}$ values are closer to the measured T_{se} than T_e because of solar warming. However, as inferred from Eq. (1), a difference of several degrees centigrade between $T_{sol\text{-}air}$ and T_{se} can exist for large values of $q_e R_{se}$.

5.2. Numerical calculation of the heat flux and temperature through the wall

a) *Considering a sinusoidal variation of the external temperature*

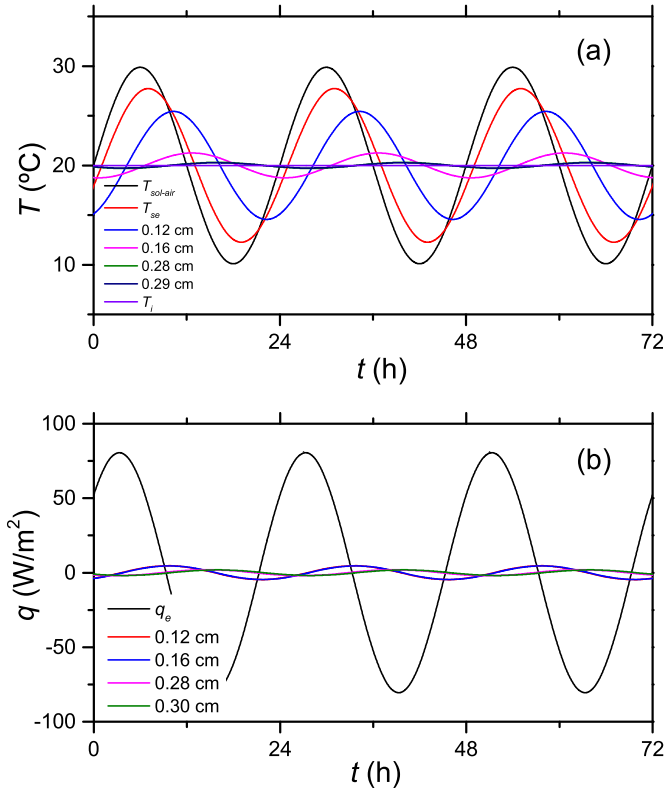

Fig. 4. Evolution of the temperature (a) and heat flux (b) in the interfaces between the different layers that compose the wall when T_e varies in a sinusoidal way.

To determine the dynamical response of the wall, the temperature distribution inside it is simulated numerically when the wall is exposed to a temperature $T_{\text{sol-air}}$ that varies in a sinusoidal way with period $\tau = 24$ h and amplitude of 10 °C from a mean value of 20 °C and $T_i = 20$ °C = const. Then, the results are compared with those obtained with the admittance method (Section 3.2).

After having achieved the solution $T(x,t)$, the flux $q(x,t)$ is calculated using Eq. (7). Fig. 4 shows the evolution of the temperature (Fig. 4a) and heat flux (Fig. 4b) through the internal interfaces of the wall sketched in Fig. 5a. As expected, Fig. 4a shows significant differences between the evolution of $T_{\text{sol-air}}$ (black line), T_{se} (red line), the temperature at $x = 0.12$ m (between the solid brick and the EPS – blue line) and the temperature at $x = 0.16$ m (between the EPS and the hollow brick – magenta line) because of the notable change of the properties (i.e. ρ, C_p, λ) of the materials located on both sides of the respective interface. As a result, the temperatures in the internal edge of the hollow brick ($x = 0.28$ m) and in the plasters almost equal T_i. Furthermore, Fig. 4b shows that the heat flux q_e exchanged between the exterior and the wall (black line) is important; this effect creates the difference between the $T_{\text{sol-air}}$ and T_{se} curves observed in Fig. 4a. From the external surface ($x/\ell = 0$), $q(x)$ varies continuously throughout the wall (green-dotted line in Fig. 5b), basically because of energy conservation, with an appreciable decrease up to the first internal interface. Consequently, only a small fraction of q_e is transmitted into the interior. This heat exchange differs significantly from that attained when a steady-state flux is considered as represented by the green solid line in Fig. 5b.

Another issue to note is the time difference between the temperature variations on the internal and external wall sides, and between the temperature and heat flux variations. These phase shifts result from the dynamical thermal response of a multi-layer wall, such as the one analysed here. The evolution of the maximum temperature position is shown by the solid magenta line in Fig. 6. This figure shows that the maximum values that correspond to different positions x inside the wall are not reached at the same time, as would occur in the steady-state case. By contrast, there is a time lag of about 10 h between the times in which the maximum is achieved at $x = 0$ and $x = \ell$.

Then, the wall dynamical parameters are estimated. The admittance of a material is its ability to exchange heat with the surrounding environment under cyclical temperature variations. It is determined by means of the following:

$$Y = \frac{\max(q_e)}{T_{\text{sol-air}}|_{\max} - T_{\text{sol-air}}|_{\min}} \cos(\varphi_Y), \tag{12}$$

where φ_Y is the time lag between the temperature and the heat flux evolution on the external wall side. Similarly, the dynamical transmittance is defined as follows:

$$u = \frac{\max(q_i)}{\max(T_{\text{sol-air}} - T_i)} \cos(\varphi), \tag{13}$$

where φ is the time lag between a peak in the outdoor temperature $T_{sol\text{-}air}$ and the corresponding peak in the heat flux released to the indoor air q_i. In addition, the decrement factor:

$$f = \frac{u}{U} = \frac{q_i}{q_{ss}}, \tag{14}$$

provides the reduction of the periodic variations of the heat flux through the wall regarding the steady-state flux $q_{ss} = (T_{\text{sol-air}} - T_i)/R_t$.

Table 5 shows that the dynamical parameters calculated from the numerical results using Eqs. (12)–(14) are very similar to those obtained with the admittance method [41]. From this comparison, and from the comparison between analytical and numerical results (not shown here), the numerical solution of the heat equation properly represents the heat transfer considered.

b) *Considering real external temperature variations*

The next step is to solve Eq. (3) numerically when the wall sides are exposed to temperatures $T_{\text{sol-air}}$ and T_i. The temperature $T(x,t)$ and heat flux $q(x,t)$ obtained in the entire domain for one of the intervals analysed are shown in Fig. 7. As highlighted in Section 5.2a, the heat flux through the wall evolves differently from that in the steady-state. On the contrary, $q(x,t)$ depends on the temperature distribution and evolution inside the walls. Consequently, the extreme maximum and minimum values of $q(x,t)$ are observed (Fig. 7b); this highlights the intense heat exchange between the external wall surface and its surroundings. During the day, the wall absorbs a large amount of heat due to solar radiation, which is revealed in the great difference between $T_{\text{sol-air}}$ and T_e (Fig. 7a). Such an amount of heat is given back to the environment during the night, as evidenced by the q_e minima observed in Fig. 7b.

Once q_e has been determined, T_{se} is calculated instant by instant by means of Eq. (1). When the environment delivers heat to the wall ($q_e > 0$), it results in $T_{se} < T_{\text{sol-air}}$. When the flux is at its maximum (Fig. 7b), temperature differences of up to 6 °C are reached. On the contrary, when the wall delivers heat to the environment, it results in $T_{se} > T_{\text{sol-air}}$ and the temperature difference reaches about 4 °C when the flux is at its minimum (Fig. 6b). The maximum and minimum of q_e vary according to season. The $T_{\text{sol-air}} - T_{se}$ value can reach up to 8 °C at midday in spring and autumn, and up to −6 °C during the winter nights as shown in Fig. 8. The T_{se} values calculated in this way are successfully compared with those measured by using IRT in Fig. 9.

6. Remarks

As observed in Fig. 3, the surface temperature T_{se} of the walls exposed to direct solar radiation increases to a value that is

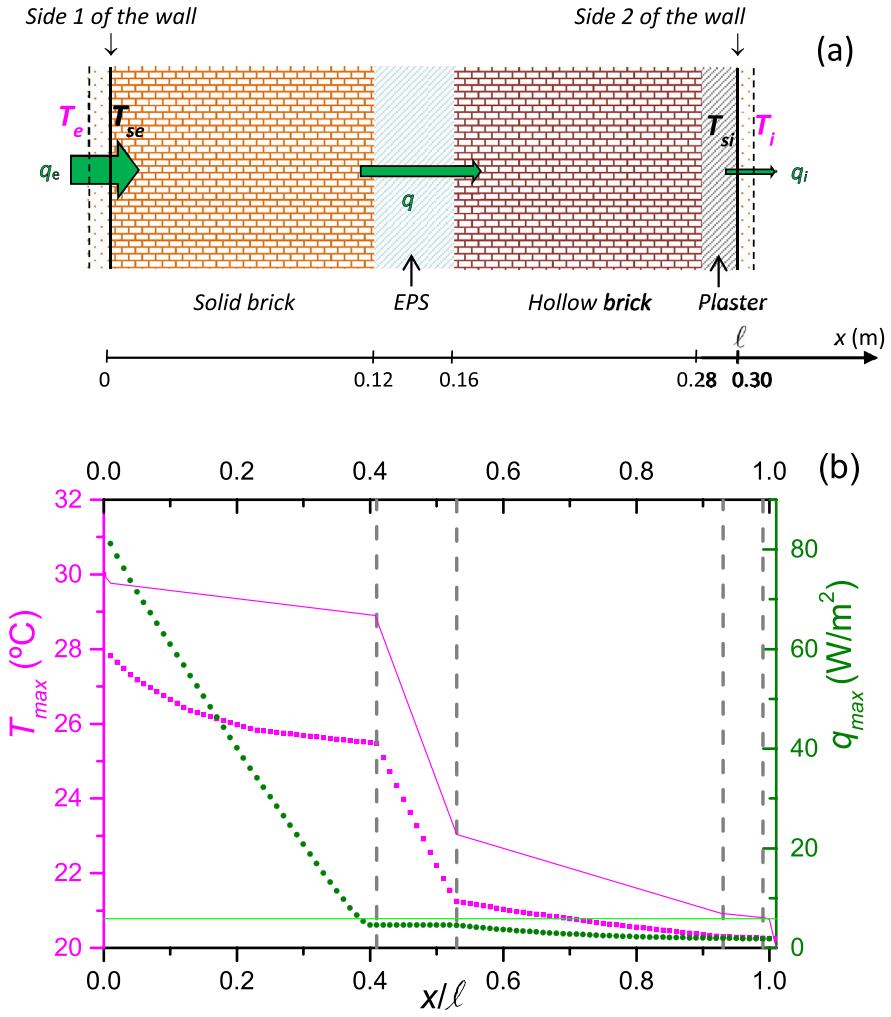

Fig. 5. (a) Sketch of the wall. (b) Spatial profiles of the maximum temperature (magenta-dotted lines) and heat flux (green-dotted lines) resulting from numerical simulation and the corresponding analytical solutions for the steady-state regime (solid lines). (For interpretation of the references to colour in this figure legend, the reader is referred to the web version of this article.)

Table 5
Validation of the dynamical parameters of the assessed wall.

	Y (W/m^2 °C)	f	φ (h)	u (W/m^2 °C)
Numerical results and Eqs. (12)–(14)	3.7	0.33	10	0.19
Admittance method	3.9	0.32	10	0.17

much greater than T_e. An external temperature T_e in the range 10 °C–27 °C in spring and autumn, which is typical of temperate climates, implies an equivalent surface temperature $T_{\text{sol-air}}$ of up to 45 °C when the incident solar radiation is considered (Fig. 3b,c). In summer and winter, the situation is critical because of the high external temperatures and solar radiation on the vertical walls, respectively. This causes an important increase of the heat flux into the interior, which must be considered in the calculation of heat gains and losses by conduction through the envelope. As shown in Section 5, it is possible to calculate the surface temperature of the walls exposed to a high solar radiation at different times of the day and seasons, and compare them with the in situ thermographic measurements, hence obtaining a satisfactory agreement. This kind of measurement takes advantage of the air's transparency to the infrared radiation emitted by the surfaces over short distances, thus enabling the collection of information that is difficult to acquire with other means.

The developed methodology combines the measured temperature T_e and the total irradiance I_t incident on the surface of interest (in this case, a vertical wall facing northeast) by means of the temperature $T_{\text{sol-air}}$ and the resistance R_{se} of the external air boundary layer. From these data and the measured temperature T_i, the flux q_e through the wall is obtained by numerically solving the heat Eq. (3). As a result, this thermal flux introduces a temperature difference $T_{\text{sol-air}} - T_{se}$ that is an indicative of the impact of the solar radiation on the real heat transferred into the building. Alternatively, from Eq. (2), $T_{\text{sol-air}}$ can be calculated by employing the intensity of the instantaneous solar radiation measured at a near weather station. For the wall considered here, the T_{se}-values calculated in this way would also achieve a general agreement with the thermographic measurements although the dispersion of the points would be like that of Fig. 9. The dispersion of the experimental points in Fig. 9 can be explained partly by the difference between the solar radiation intensity, whether calculated or measured at the weather station, and that effectively absorbed by the

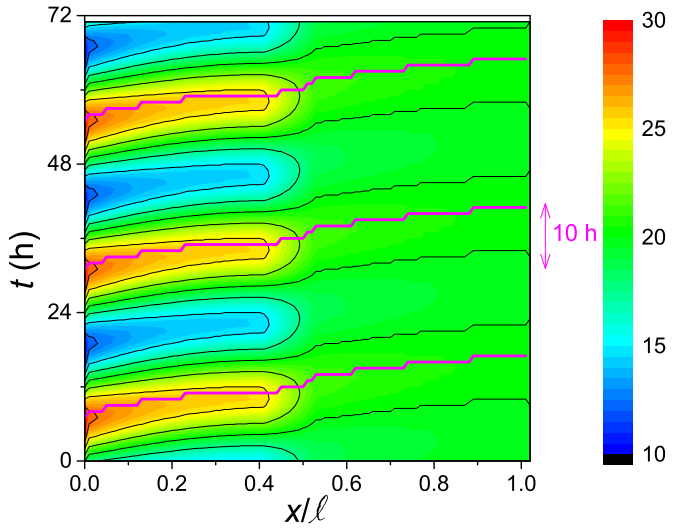

Fig. 6. Contour plot of the temperature distribution. The magenta lines represent the position of the maximum temperatures as a function of time. (For interpretation of the references to colour in this figure legend, the reader is referred to the web version of this article.)

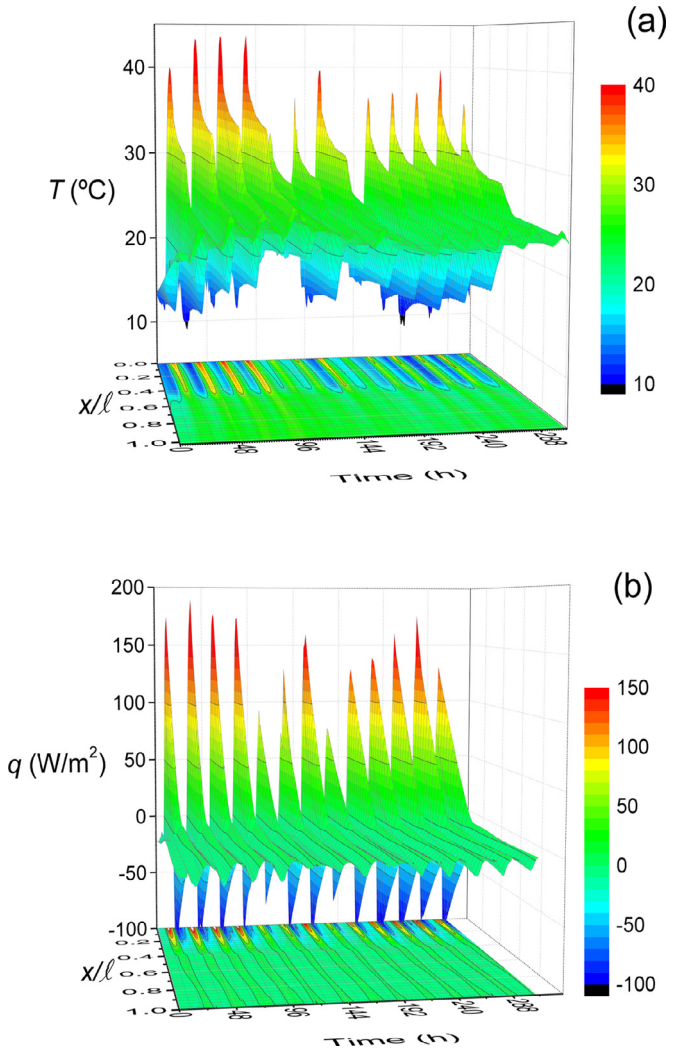

Fig. 7. Spatial-temporal distribution of (a) temperature and (b) heat flux corresponding to the interval between 29 March and 7 April 2016 (autumn).

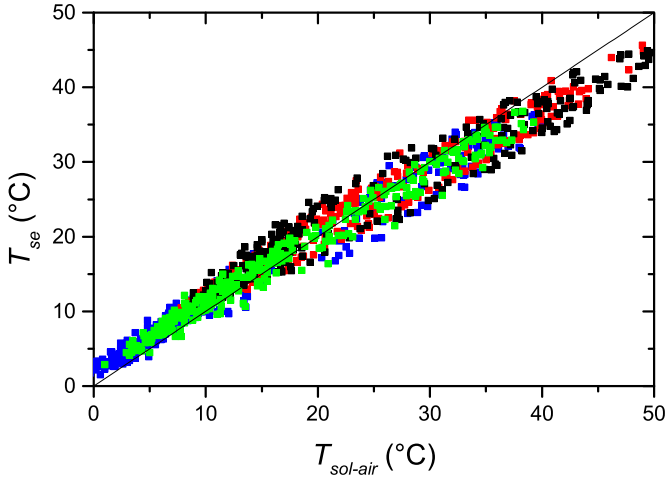

Fig. 8. External surface temperature numerically calculated as a function of the sol-air temperature in the intervals 19–30 October 2015 (green symbols), 29 March to 7 April 2016 (black symbols), 4–15 July 2016 (blue symbols) and 29 November to 7 December 2016 (red symbols). The line $T_{se} = T_{sol\text{-}air}$ is added for comparison. (For interpretation of the references to colour in this figure legend, the reader is referred to the web version of this article.)

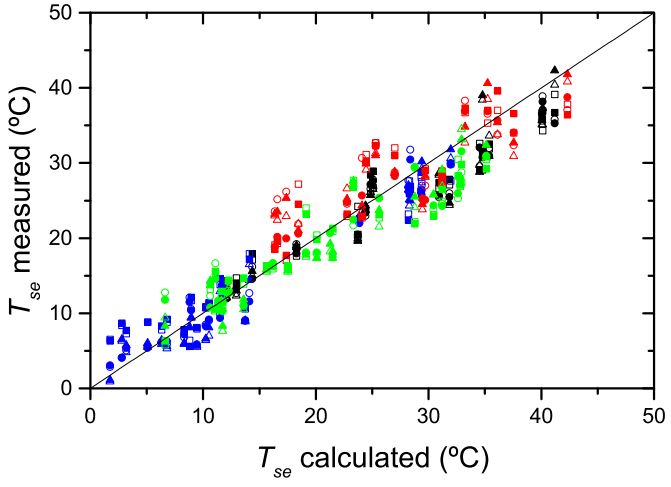

Fig. 9. External surface temperature measured with the thermographic camera as a function of what was calculated from $T_{sol\text{-}air}$ and q_e obtained numerically. Colours are coded in the same way as in Fig. 7. (■: W1-GF, □: W1UF, ●: W2GF, ○: W2UF, ▲: W3Gf, △: W3Uf). The line $T_{se)measured} = T_{se)calculated}$ is added for comparison.

wall. In fact, the I_t-value at a time proximate to that of the thermographic measurement does not account for the irradiance evolution, and this is important to consider when a wall with a high thermal inertia is evaluated. In addition, possible variations of h_e also influence the dispersion of the points in Fig. 9. These variations are due to changes in the wind intensity and direction, temperature, humidity, shape of the envelope and surrounding obstacles (e.g. trees, other buildings), which are difficult to take into account properly.

The determination of q_e by solving numerically the non-steady-state heat equation and using the real internal and external temperatures (in addition to the total irradiance) is critical for obtaining T_{se} correctly, especially when walls with a high thermal inertia are analysed. Even when the *MATLAB* simulation code is used, which is simple and easy to programme, other codes and subroutines in Fortran, *C++* and other languages are available to solve Eq. (3) with the BC given by (1) and (10). There is also commercial software for numerically solving the differential equations associated with the heat transfer through the building envelope.

These software use different methods, such as the explicit [46] or implicit [47] finite difference schemes, finite element method [48], implicit [49] or explicit [50] finite volume schemes, spectral method [51], and other methods based on analogies with thermal circuits [52], transfer functions [53] and so forth. Other methods or schemes to approximate the temporal derivative can obtain a better resolution and/or be more efficient computationally; however, they can require a greater amount of programming knowledge. Here, the code is not important, only its correct use knowing its limitations and errors.

Usually, Eq. (4) is used to determine the heat transfer through a homogeneous medium. In this case, the behaviour of the medium is described by the thermal diffusivity that relates the thermal conductivity, density and specific heat of the material. If the medium is non-homogeneous, λ and ρC_p must be considered separately, as in Eq. (3). Both parameters determine the correct thermal behaviour of every layer and, ultimately, of the entire wall. Then, the standard simulation codes that are prepared to solve the classic Eq. (4) must be modified. Otherwise, the heat flux through the different internal interfaces does not fulfil Eq. (7), or it does so with a big error, and wrong results can be obtained if the thermal characteristics of the wall layers are significantly different.

Another critical point of the numerical simulation is the choice of the BC and IC. The air boundary layers of the internal and external wall surfaces are considered by means of the corresponding convective coefficients or, equivalently, by means of the surface thermal resistances. Thus, it is possible that $T_{sol\text{-}air}$ or T_i matches with the surface temperatures, reaching the heat flux conservation in the boundary layers despite the different thermal properties of the air and wall.

7. Conclusions

The main contribution of the current research is the development of a new methodology to obtain the external surface temperature of walls – validated by in situ measurements – at any moment of the day in any season of the year. The results are successfully compared to measurements performed applying IRT, while the procedure highlights valuable physical information on the heat transfer by conduction through the building envelope. The number of measurements conducted at different days and times compensate for the statistical fluctuations, hence enabling a reasonable correlation between theory and in situ measurements. Thus, the solar radiation effects on the heat transfer through the building envelope can be considered, while the parameters related to the $T_{\text{sol-air}}$ calculation (see Table 2) can be experimentally validated at the construction's specific location. This methodology can be extended to the assessment of walls with partial exposure to solar radiation such as, for example, walls with parasols or surrounding vegetation.

The theoretical calculation of the surface temperature requires knowing the evolution of the air external temperature T_e, the total incident solar radiation I_t on the wall and the external surface thermal resistance R_{se} of the air boundary layer. From these values, the heat flux is determined by numerically solving Eq. (3) and considering the evolution of internal T_i and equivalent external $T_{\text{sol-air}}$ temperatures. In addition, the results improve the understanding of the dynamical response of the different layers that compose the wall and the contribution of these layers to the global thermal behaviour of the wall. The procedure also evinces the large amount of heat absorbed by the wall, which indirectly contributes to the formation of urban heat islands. The problem addressed is an interesting application of the solution of the heat flux equation through non-homogeneous media, with the BC involving the air boundary layers adjacent to rigid contours, and on how to get relevant physical information about the processes related to heat conduction through thermal interfaces.

Finally, by measuring the external and internal surface temperatures of a wall and knowing the thermal characteristics of the construction materials, the heat flux and surface resistances can be calculated following, for example, Marino et al. [27]. From here, the heat losses by conduction through the building envelope can be quantified, and the design parameters values can be corroborated by means of in situ measurements, as in the present study.

References

[1] C.S. Barnaby, J.L. Wright, M.R. Collins, Improving load calculations for fenestration with shading devices, ASHRAE Tran. 115 (2009) 31–44 RP-1311. *UWSpace*, http://hdl.handle.net/10012/11548.
[2] S.F. Bruning, Load calculation spreadsheets: quick answers without relying on rules of thumb, ASHRAE J. 54 (2012) 40–45.
[3] S. Sansregret, K. Lavigne, Spreadsheet tool development for visualizing building performance and simulation data to help calibrating models, ASHRAE/IBPSA-USA Building Simulation Conference, 2014.
[4] A.C. Menezes, A. Cripps, D. Bouchlaghem, R. Buswell, Predicted vs. actual energy performance of non-domestic buildings: using post-occupancy evaluation data to reduce the performance gap, Appl. Energy 97 (2012) 355–364.
[5] O. Guerra-Santín, C. Tweed, H. Jenkins, S. Jiang, Monitoring the performance of low energy dwellings: two UK case studies, Energy Build. 64 (2013) 32–40.
[6] P. De Wilde, The gap between predicted and measured energy performance of buildings: a framework for investigation„ Automat. Constr. 41 (2014) 40–49.
[7] R. Kumar, S.C. Kaushik, Performance evaluation of green roof and shading for thermal protection of buildings, Build. Environ. 40 (2005) 1505–1511.
[8] A. Tzempelikos, A.K. Athienitis, The impact of shading design and control on building cooling and lighting demand, Sol. Energy 81 (2007) 369–382.
[9] V.C. Kapsalis, E. Vardoulakis, D. Karamanis, Simulation of the cooling effect of the roof added photovoltaics, Adv. Build. Energy Res. 8 (2014) 41–54.
[10] G. Huelsz, G. Barrios, J. Rojas, Differences on results from steady-state and time-dependent wall/roof heat transfer models in Mexican climates, Energy Procedia 57 (2014) 1825–1833.
[11] C. Yan, S. Wang, K. Shan, Y. Lu, A simplified analytical model to evaluate the impact of radiant heat on building cooling load, Appl. Therm. Eng. 77 (2015) 30–41.
[12] T. Aoki, A. Mizutani, Measurement of the vertical distribution of reflected solar radiation, J. Eng. Technol. Sci. 47 (2015) 160–169.
[13] R. Albatici, A.M. Tonelli, Infrared thermovision technique for the assessment of thermal transmittance value of opaque building elements on site, Energy Build. 42 (2010) 2177–2183.
[14] P.A. Fokaides, S.A. Kalogirou, Application of infrared thermography for the determination of the overall heat transfer coefficient (U-Value) in building envelopes, Appl. Energy 88 (2011) 4358–4365.
[15] R. Albatici, A.M. Tonelli, M. Chiogna, A comprehensive experimental approach for the validation of quantitative infrared thermography in the evaluation of building thermal transmittance, Appl. Energy 141 (2015) 218–228.
[16] B. Tejedor, M. Casals, M. Gangolells, X. Roca, Quantitative internal infrared thermography for determining in-situ thermal behaviour of façades, Energy Build. 151 (2017) 187–197.
[17] R. Albatici, F. Passerin, A.M. Tonelli, S. Gialanella, Assessment of the thermal emissivity value of building materials using an infrared thermovision technique emissometer, Energy Build. 66 (2013) 33–40.
[18] K. Gaspar, M. Casals, M. Gangolells, A comparison of standardized calculation methods for in situ measurements of facades U-value, Energy Build. 130 (2016) 592–599.
[19] T.H. Kuehn, W.W. Ramsey, J.L. Threlkeld, in: Thermal Environmental Engineering„ 481-485, Prentice Hall, New Jersey, 2001, pp. 559–560.
[20] S.A. Kalogirou, G. Florides, S. Tassou, Energy analysis of buildings employing thermal mass in Cyprus, Renew. Energy 27 (2002) 353–368.
[21] J. Zhou, G. Zhang, Y. Lin, Y. Li, Coupling of thermal mass and natural ventilation in buildings, Energy Build. 40 (2008) 979–986.
[22] H. Janssen, B. Blocken, J. Carmeliet, Conservative modelling of the moisture and heat transfer in building components under atmospheric excitation, Int. J. Heat Mass Tran. 50 (2007) 1128–1140.
[23] U.M. Karmele, M.G. Davies, One-dimensional solutions to Fourier's equation and measurements of heat transmission through walls: The role of wall decay times, Build. Environ. 43 (2008) 1433–1445.
[24] M. Qin, R. Belarbi, A. Ait-Mokhtar, L.O. Nilsson, Coupled heat and moisture transfer in multi-layer building materials, Constr. Build. Mater. 23 (2009) 967–975.
[25] L.A. Pipes, Matrix analysis of heat transfer problems, J. Franklin Inst. 623 (1957) 195–206.
[26] M.G. Davis, The thermal response of an enclosure to periodic excitation: the CIBSE approach, Build. Environ. 29 (1994) 217–235.
[27] B.M. Marino, N. Muñoz, L.P. Thomas, Estimation of the surface thermal resistances and heat loss by conduction using thermography, Appl. Therm. Eng. 114 (2017) 1213–1221.

[28] E. Grinzato, N. Ludwig, G. Cadelano, M. Bertucci, M. Gargano, P. Bison, Infrared thermography for moisture detection: a laboratory study and in-situ test, Mater. Eval. 69 (2011) 97–104.
[29] E. Lucchi, Applications of the infrared thermography in the energy audit of buildings: a review, Renew. Sust. Energ. Rev. 82 (Part 3) (2018) 3077–3090.
[30] A. Kylili, P.A. Fokaides, P. Christou, S.A. Kalogirou, Infrared thermography (IRT) applications for building diagnostics: a review„ Appl. Energy 134 (2014) 531–549.
[31] G. Dall'O', L. Sarto, A. Panza, Infrared screening of residential buildings for energy audit purposes: results of a field test„ Energies 6 (2013) 3859–3878.
[32] International Organization for Standardization, EN 13187:1998 (ISO6781:1983 Modified, Thermal performance of buildings. qualitative detection of thermal irregularities in building envelopes, Infrared Method (1998).
[33] I. Nardi, S. Sfarra, D. Ambrosini, Quantitative thermography for the estimation of the U-value: state of the art and a case study, J. Phys. Conf. Ser. 547 (2014) 012016.
[34] I. Danielski, M. Fröling, Diagnosis of buildings' thermal performance. a quantitative method using thermography under non-steady state heat flow, Energy Procedia 83 (2015) 320–329.
[35] L. Evangelisti, C. Guattari, P. Gori, F. Bianchi, Heat transfer study of external convective and radiative coefficients for building applications, Energy Build. 151 (2017) 429–438.
[36] M. O'Grady, A.A. Lechowska, A.M. Harte, Quantification of heat losses through building envelope thermal bridges influenced by wind velocity using the outdoor infrared thermography technique, Appl. Energy 208 (2017) 1038–1052.
[37] P.W. O'Callaghan, S.D. Probert, Sol-air temperature, Appl. Energy 3 (1977) 307–311.
[38] C. Peng, Z. Wu, In situ measuring and evaluating the thermal resistance of building construction, Energy Build. 40 (2008) 2076–2082.
[39] ASHRAE. ASHRAE Handbook – Fundamentals., Atlanta: American Society of Heating, Refrigerating and Air-Conditioning Engineers Inc, 2009.
[40] J.W. Spencer, Fourier series representation of the position of the sun, Search 2 (1971) 172–173.
[41] N. Muñoz, L.P. Thomas, B.M. Marino, Comportamiento térmico dinámico de muros típicos empleando el método de la admitancia, Energías Renovables y Medio Ambiente 36 (2015) 31–39.
[42] M. Hazewinkel, Parabolic Partial Differential Equation, Numerical Methods, Encyclopaedia of Mathematics, Springer, 2001.
[43] L.F. Shampine, I. Gladwell, S. Thompson, Solving ODEs with matlab. Cambridge University Press, 2003.
[44] L.F. Shampine, J. Kierzenka, M.W. Reichelt, Solving boundary value problems for ordinary differential equations in MATLAB with bvp4c, 2000. URL 2000 http://www.mathworks.com/matlabcentral/fileexchange/3819.
[45] J.W. Thomas, Numerical partial differential equations: finite difference methods, Texts in Applied Mathematics, 22, Springer-Verlag, New York, 1995.
[46] H. Asan, Y. Sancaktar, Effects of Wall's thermophysical properties on time lag and decrement factor, Energy Build. 28 (1997) 159–166.
[47] M. Ozel, K. Pihtili, Optimum location and distribution of insulation layers on building walls with various orientations, Build. Environ. 42 (2007) 3051–3059.
[48] C. Chen, E. Krokosky, Steady and non-steady solar heat transmission through roofs„ Mater. Struct. 9 (1976) 19–32.
[49] S. Al-Sanea, Finite-volume thermal analysis of building roofs under two-dimensional periodic conditions, Build. Environ. 38 (2003) 1039–1049.
[50] G. Barrios, G. Huelsz, J. Rojas, Thermal performance of envelope wall/roofs of intermittent air-conditioned rooms, Appl. Therm. Eng. 40 (2012) 1–7.
[51] D. Gottlieb, S. Orzag, Numerical Analysis of Spectral Methods: Theory and Applications, SIAM, Philadelphia, 1977.
[52] K. Kontoleon, D. Bikas, The effect of south wall's outdoor absorption coefficient on time lag, decrement factor and temperature variations, Energy Build. 39 (2007) 1011–1018.
[53] A. Gasparella, G. Pernigotto, M. Baratieri, P. Baggio, Thermal dynamic transfer properties of the opaque envelope: Analytical analytical and numerical tools for the assessment of the response to summer outdoor conditions, Energy Build. 43 (2011) 2509–2517.